Sigma-Aldrich®
Lab & Production Materials

Application Note

Analysis of Ionic Conductivity and Electrochemical Behavior of Lithium Salts

Manasi Mwemezi[1], Jun Choi[1], Amir Chamaani[2]
[1]R&D and Customer Support Lab APAC (Daejeon, South Korea)
[2]Energy Storage and Battery Materials, Materials Science R&D (Milwaukee, WI, USA)

Abstract

This study highlights the electrochemical performance and practical application considerations of widely used lithium salts, including lithium hexafluorophosphate ($LiPF_6$), lithium bis(fluorosulfonyl)imide (LiFSI), and their mixed-salt formulations. A comprehensive electrochemical evaluation of ionic conductivity, lithium-ion transference number, coulombic efficiency, lithium metal plating/stripping behavior, aluminum compatibility, and oxidative stability provides clear insight into how salt selection influences electrolyte performance. The results reveal distinct strengths and trade-offs among the evaluated formulations, enabling targeted optimization of transport efficiency, lithium metal reversibility, and anodic stability. These findings offer users a data-driven guide on selecting and tailoring electrolyte salt compositions using proven, commercially available materials to meet diverse battery performance and reliability requirements.

Figure 1. Spider chart comparing characteristics of electrolytes with $LiPF_6$, LiFSI, and mixed-salt electrolytes.

Introduction

The performance of lithium-ion batteries is significantly influenced by the physicochemical properties of the electrolyte, particularly the choice of lithium salt and its interactions with the solvent, current collectors, and electrode interfaces. Among commercially relevant electrolytes, lithium hexafluorophosphate ($LiPF_6$) in ethylene carbonate/dimethyl carbonate (EC/DMC) has long been the industry standard due to its balanced ionic conductivity, ability to form stable passivation layers on aluminum, and compatibility with layered oxide cathodes.[1,2] However, $LiPF_6$ is inherently unstable in the presence of moisture, thermally-unstable, and prone to generating hydrofluoric acid (HF) and phosphorus pentafluoride (PF_5). These issues can lead to continuous parasitic reactions, gas formation, and long-term performance degradation.[3,4]

In contrast, lithium bis(fluorosulfonyl)imide (LiFSI) has emerged as a promising next-generation salt, offering high ionic-dissociation, superior low-temperature performance, and enhanced ionic conductivity in carbonate solvents. The FSI^- anion facilitates the formation of robust, LiF-rich interphases that can improve lithium metal plating morphology and coulombic efficiency.[5–7] However, LiFSI poses a significant challenge due to its tendency to corrode aluminum at high potentials, which can result in current collector pitting or loss of passivation unless stabilized through co-salts and/or additives.[8–10] To balance these attributes, mixed-salt or dual-salt electrolytes that combine $LiPF_6$ and LiFSI are increasingly used to couple improved transport and interphase formation with aluminum passivation. Thus, understanding the interplay between $LiPF_6$ and LiFSI whether synergistic or detrimental remains a critical research direction for developing stable electrolytes in both lithium-metal and high-voltage lithium-ion systems.

This study presents a comparative evaluation of $LiPF_6$- and LiFSI-based electrolyte salts and their mixtures, designed to guide customers in selecting formulations that best match targeted performance and stability requirements.

The Life Science business of Merck operates as MilliporeSigma in the U.S. and Canada.

MERCK

Experimental

Materials

Lithium salts ($LiPF_6$ and LiFSI), electrolyte solvents (EC and DMC), stainless steel (SS), platinum (Pt), anhydrous ethanol and acetone were internally sourced. All materials were used as received, without further purification or drying.

Electrolyte solvents were mixed in a volume ratio of EC:DMC = 30:70. Electrolytes were prepared by dissolving lithium salts to obtain a total lithium-ion concentration of 1.0 M, with the following concentrations:

- 1.0 M $LiPF_6$
- 0.9 M $LiPF_6$ + 0.1 M LiFSI
- 0.8 M $LiPF_6$ + 0.2 M LiFSI
- 0.5 M $LiPF_6$ + 0.5 M LiFSI
- 1.0 M LiFSI

The resulting electrolyte formulations were stirred for 4 hours prior to use to ensure complete dissolution and homogeneity.

Copper (Cu), aluminum (Al), stainless steel (SS), platinum (Pt), and lithium (Li) metal were used as electrode materials. Cu foils were cut into circular discs with a diameter of 16 mm and treated with 1 M HCl, followed by sequential washing in acetone and anhydrous ethanol via sonication for 15 minutes to remove surface impurities and native oxide layers. Aluminum foils were cut into 16 mm circular discs and used as received.

All cells were assembled in an argon-filled glovebox, using lithium metal as the counter and reference electrode where applicable.

Materials Characterization

The surface morphology of the aluminum foils after 5 cyclic voltammetry (CV) cycles was examined using scanning electron microscopy (SEM, HITACHI SU8700) to assess surface features relevant to aluminum corrosion behavior and electrolyte–current collector interactions.

Electrochemical Characterization

Electrochemical measurements were performed at 25 °C using CR2032 coin cells assembled with Celgard trilayer PP/PE/PP separators, except where otherwise specified.

Ionic conductivity (σ) was measured using a dedicated conductivity cell containing two parallel stainless-steel electrodes with known electrode area (A) and separation distance (L). The solution resistance (R) was obtained from electrochemical impedance spectroscopy (EIS), and ionic conductivity was calculated using the formula:

$$\sigma = \frac{L}{RA}$$

Lithium-ion transference (t_{Li^+}) numbers were determined in Li|electrolyte|Li symmetric cells using the Bruce–Vincent method,

$$t_{Li^+} = \frac{I_{ss}\,(V - I_O R_O)}{I_O\,(V - I_{SS} R_{SS})}$$

with lithium metal disks serving as both working and counter electrodes.[11] For each electrolyte, four independent cells were prepared and measured to ensure reproducibility. Cells were allowed to rest at open-circuit voltage for 24 hours prior to measurement to ensure interfacial stabilization. A 10 mV DC polarization was applied, and EIS spectra were collected before and after polarization. Open-circuit voltage stability was verified prior to testing.

Lithium plating/stripping coulombic efficiency (CE) was evaluated in Li|Cu cells under galvanostatic conditions, while long-term lithium metal stability was assessed using Li|Li symmetric cells. Al corrosion behavior was investigated electrochemically using aluminum working electrodes. Oxidative stability was evaluated by linear sweep voltammetry (LSV) using Al, Pt, and SS as working electrodes (WE) against lithium metal.

For ionic conductivity and lithium-ion transference number measurements, the dedicated cells were assembled without a separator to eliminate additional interfacial resistance and tortuosity effects, thereby enabling a direct evaluation of intrinsic electrolyte transport properties.

Results and Discussion

Figure 2 shows the ionic conductivity of the electrolytes as a function of the $LiPF_6$/LiFSI molar ratio. The ionic conductivity increases from 10.3 mS/cm for 1.0 M $LiPF_6$ to 10.8 mS/cm at a 0.9 M $LiPF_6$ + 0.1 M LiFSI ratio and reaches a maximum of 12.1 mS/cm at 0.8 M $LiPF_6$ + 0.2 M LiFSI. A slight decrease in conductivity is observed at higher LiFSI contents, with values of 11.8 mS/cm and 11.4 mS/cm for the 0.5 M $LiPF_6$ + 0.5 M LiFSI and 1.0 M LiFSI compositions, respectively.

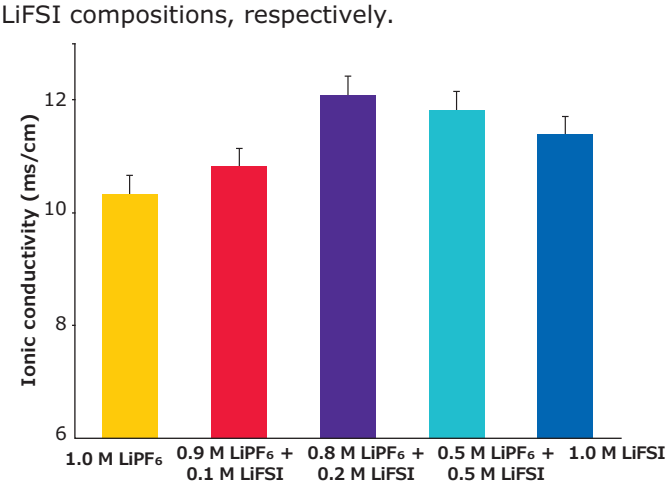

Figure 2. Ionic conductivity measurements for electrolyte solutions with varying lithium salt compositions in EC and DMC at a volume ratio of 30:70. Error bars represent the standard error of the mean (n = 5 independent experiments).

A parallel trend is observed for the lithium-ion transference number, as shown in **Figure 3**. The transference number increases from 0.29 for the 1.0 M $LiPF_6$ electrolyte to 0.34 at 0.9 M $LiPF_6$ + 0.1 M LiFSI ratio, reaching a maximum of 0.52 at the 0.8 M $LiPF_6$ + 0.2 M LiFSI composition. Further increases in LiFSI content led to a modest reduction in transference number to 0.5 and 0.46 for the 0.5 M $LiPF_6$ + 0.5 M LiFSI and 1.0 M LiFSI electrolytes, respectively. These transference numbers represent the mean ± standard error of four independent Li|electrolyte|Li cells for each composition (*n* = *4*). This non-monotonic behavior reflects the balance between enhanced salt dissociation introduced by FSI^- anions at moderate concentrations and increasing ion–ion correlations and interfacial contributions at higher LiFSI fractions.[1] The transport properties of both 1.0 M $LiPF_6$ and 1.0 M LiFSI align well with the commonly reported ranges for carbonate-based electrolytes. Notably, $LiPF_6$ demonstrates lower lithium-ion transference numbers, while LiFSI exhibits enhanced lithium-ion transport attributed to improved salt dissociation.[6,12,13]

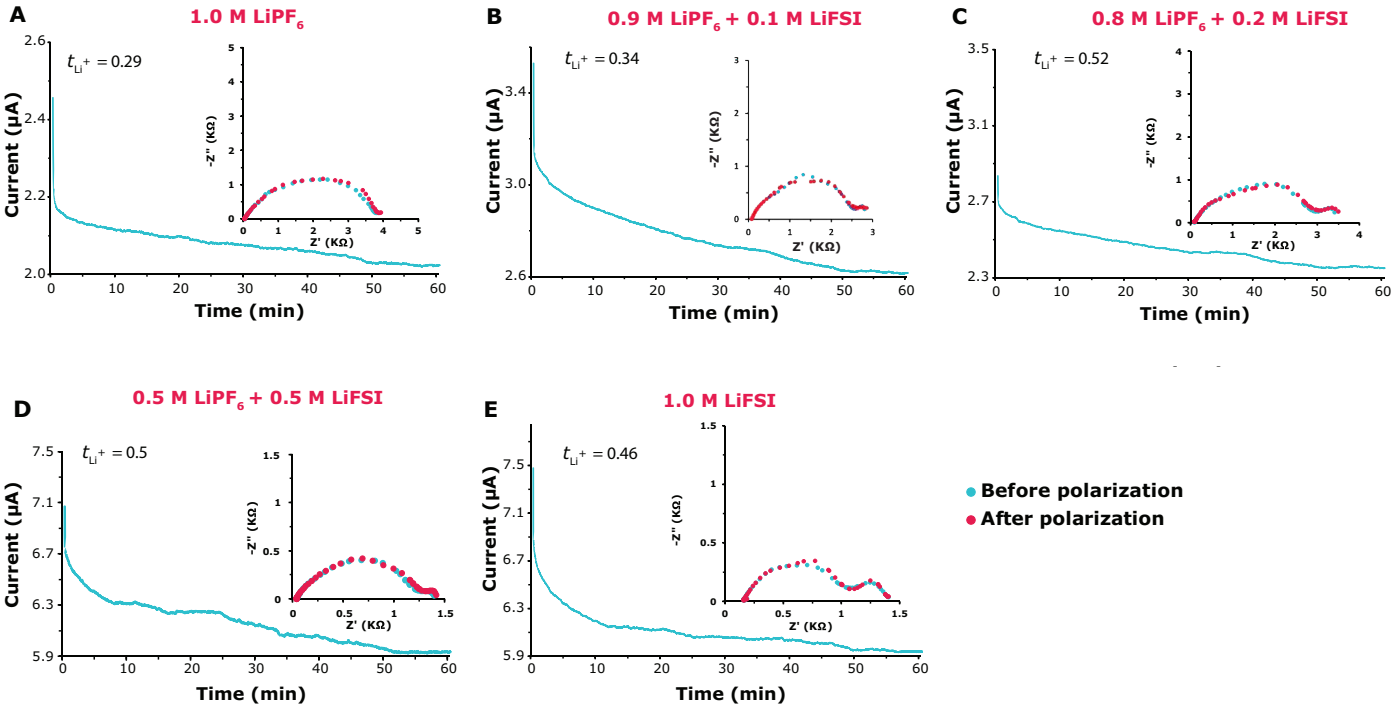

Figure 3. DC polarization profiles recorded at an applied potential of 10 mV for symmetric Li|electrolyte|Li cells containing $LiPF_6$/LiFSI mixed-salt electrolytes with molar ratios of (**A**) 1.0 M $LiPF_6$, (**B**) 0.9 M $LiPF_6$ + 0.1 M LiFSI, (**C**) 0.8 M $LiPF_6$ + 0.2 M LiFSI, (**D**) 0.5 M $LiPF_6$ + 0.5 M LiFSI, and (**E**) 1.0 M LiFSI. Insets show the corresponding EIS Nyquist plots measured before and after DC polarization.

Figure 4 illustrates that the coulombic efficiency (CE) of lithium plating/stripping in Li|Cu cells systematically increases with LiFSI content, rising from 87% for 1.0 M $LiPF_6$ to 94% for formulations containing LiFSI, indicating improved lithium reversibility and reduced parasitic reactions. In parallel, the voltage profiles reveal a clear reduction in plating/stripping overpotential for the mixed-salt and 1.0 M LiFSI, with the 0.8 M $LiPF_6$ + 0.2 M LiFSI and 0.5 M $LiPF_6$ + 0.5 M LiFSI compositions exhibiting the lowest overpotentials, consistent with enhanced interfacial kinetics.[5,6,14]

To measure CE, Li|Cu half-cell tests were performed, beginning with 10 precycles between 0 and 1 V to clean the Cu electrode surface. Lithium was then deposited at 0.5 mAh cm^{-2}, followed by stripping to 1 V. The CE was calculated as the average value over 50 consecutive cycles after the initial 10 cycles formation, by dividing the total stripping capacity by the total deposition capacity.

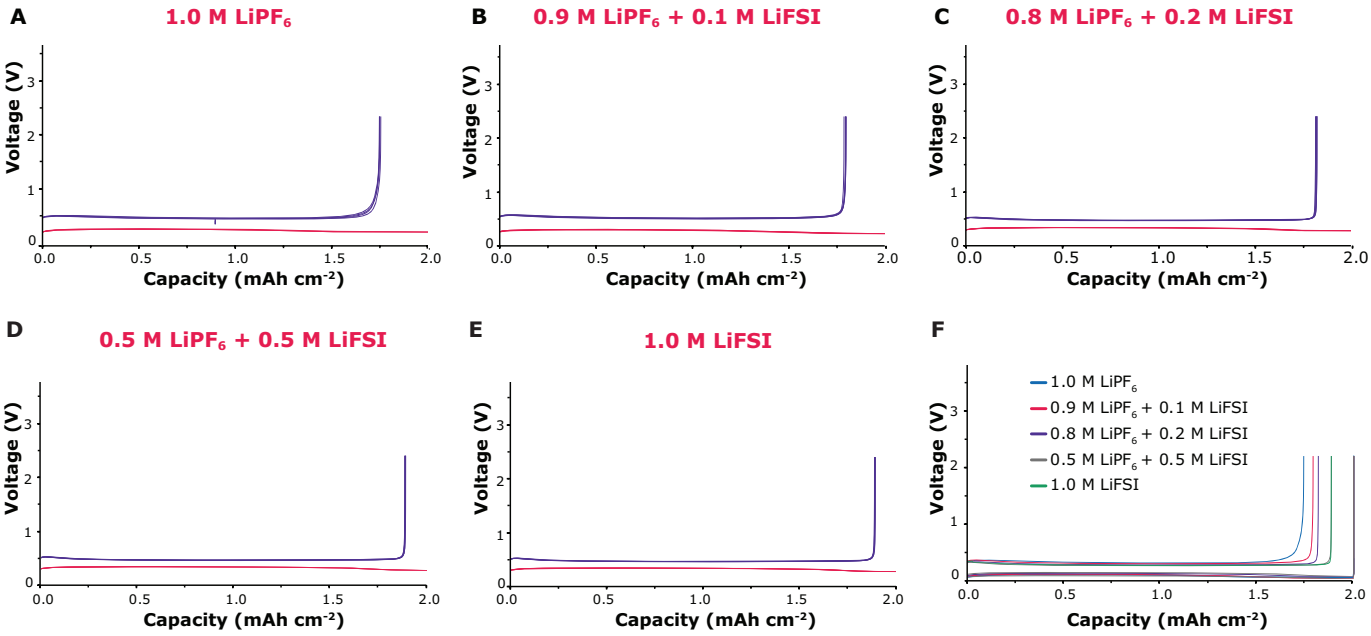

Figure 4. Li/Cu plating–stripping performance of electrolytes with different $LiPF_6$/LiFSI molar ratios: (**A**) 1.0 M $LiPF_6$, (**B**) 0.9 M $LiPF_6$ + 0.1 M LiFSI, (**C**) 0.8 M $LiPF_6$ + 0.2 M LiFSI, (**D**) 0.5 M $LiPF_6$ + 0.5 M LiFSI, and (**E**) 1.0 M LiFSI. Measurements were conducted at a current density of 0.5 mA cm^{-2} with a fixed plating capacity of 1.0 mAh cm^{-2}. CE was calculated as the average value over 50 consecutive cycles after the initial 10 cycles formation. Panel (**F**) compares the Coulombic efficiency profiles of all electrolyte compositions shown in panels (**A–E**) on a single plot for direct comparison.

Complementarily, **Figure 5** demonstrates a significant enhancement in long-term lithium metal stability. The 1.0 M $LiPF_6$ fails after approximately 120 hours, at which point the plating/stripping profile exhibits erratic voltage spikes and increased polarization, characteristic of dendrite-induced short-circuiting. In contrast, all mixed-salt electrolytes and the 1.0 M LiFSI maintain stable cycling for up to around 180 hours. Notably, even a modest incorporation of LiFSI is sufficient to achieve cycling lifetimes comparable to that of the 1.0 M LiFSI. A comparison of the representative voltage profiles in **Figure 5F** at both early and later cycles reveals differences in plating/stripping overpotentials among the electrolytes. The 1.0 M $LiPF_6$ consistently exhibits higher polarization, whereas 1.0 M LiFSI and the mixed-salt formulations show comparatively reduced and similar overpotentials, indicating lower interfacial resistance and more favorable lithium deposition behavior. The gradual increase in overpotential observed upon cycling is commonly attributed to the continuous evolution of the solid electrolyte interphase (SEI), accumulation of inactive ("dead") lithium, and progressive surface roughening at the lithium interface, all of which increase interfacial resistance over time and contribute to elevated polarization.[15–17]

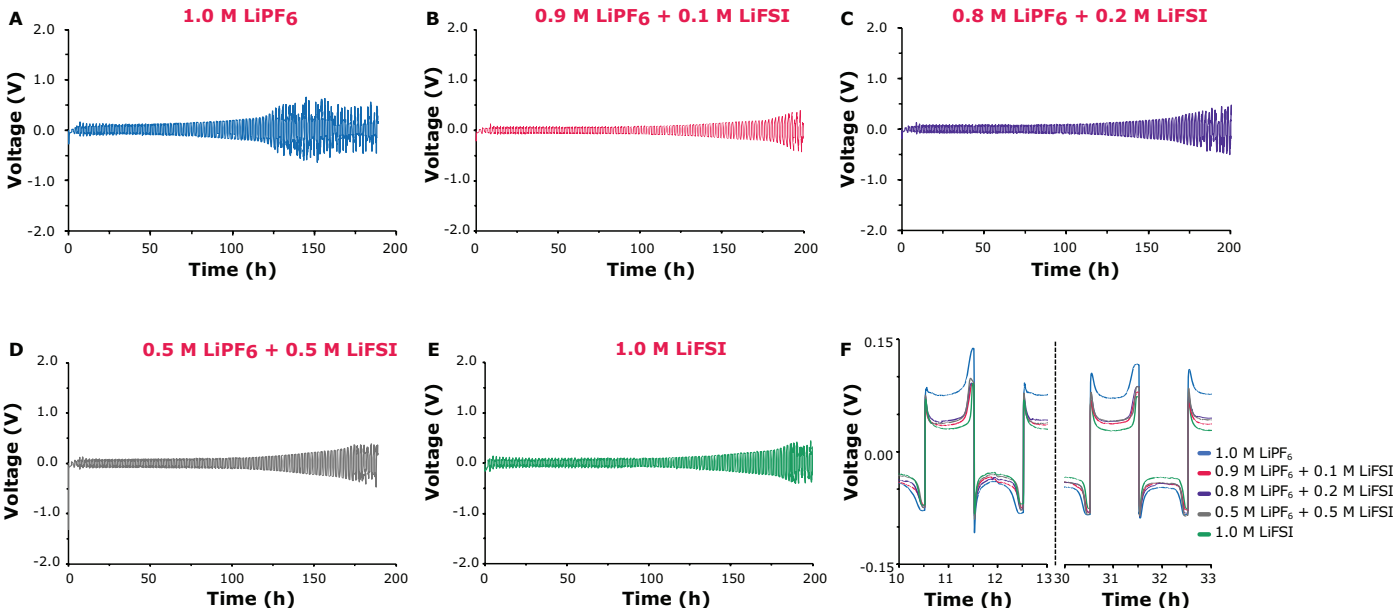

Figure 5. Galvanostatic lithium plating–stripping behavior of symmetric Li|electrolyte|Li cells containing $LiPF_6$/LiFSI electrolytes with molar ratios of (**A**) 1.0 M $LiPF_6$, (**B**) 0.9 M $LiPF_6$ + 0.1 M LiFSI, (**C**) 0.8 M $LiPF_6$ + 0.2 M LiFSI, (**D**) 0.5 M $LiPF_6$ + 0.5 M LiFSI, and (**E**) 1.0 M LiFSI, measured at a current density of 1.0 mA cm^{-2} and 1.0 mAh cm^{-2}. Panel (**F**) presents representative voltage profiles of all electrolyte compositions at cycles 10–13 and 30–33 on a single plot to enable direct comparison of plating and stripping overpotentials.

Figure 6 evaluates the aluminum corrosion behavior of the electrolytes, highlighting the trade-off between oxidative stability and interfacial reactivity. The corrosion tests were conducted using Li|electrolyte|Al coin cells, where aluminum foil served as the working electrode and lithium metal as both counter and reference electrodes. Aluminum corrosion was evaluated by cyclic voltammetry in the potential window of 3.0–5.0 V vs. Li/Li^+, with corrosion currents monitored over successive cycles to assess both the initial extent of aluminum dissolution and the stability of the passivating interphase upon continued cycling. The 1.0 M $LiPF_6$ exhibits negligible first-cycle corrosion currents and maintains very low current (<0.01 mA) during subsequent cycles, consistent with the formation of a stable, passivating AlF_3-rich layer. In contrast, LiFSI-containing electrolytes show elevated first-cycle corrosion currents, with the LiFSI-only formulation displaying pronounced initial currents exceeding 1 mA, reflecting the aggressive interaction of FSI^- anions with aluminum. Notably, mixed-salt electrolytes exhibit substantially lower first-cycle corrosion currents than 1.0 M LiFSI and show rapid current stabilization in later cycles.

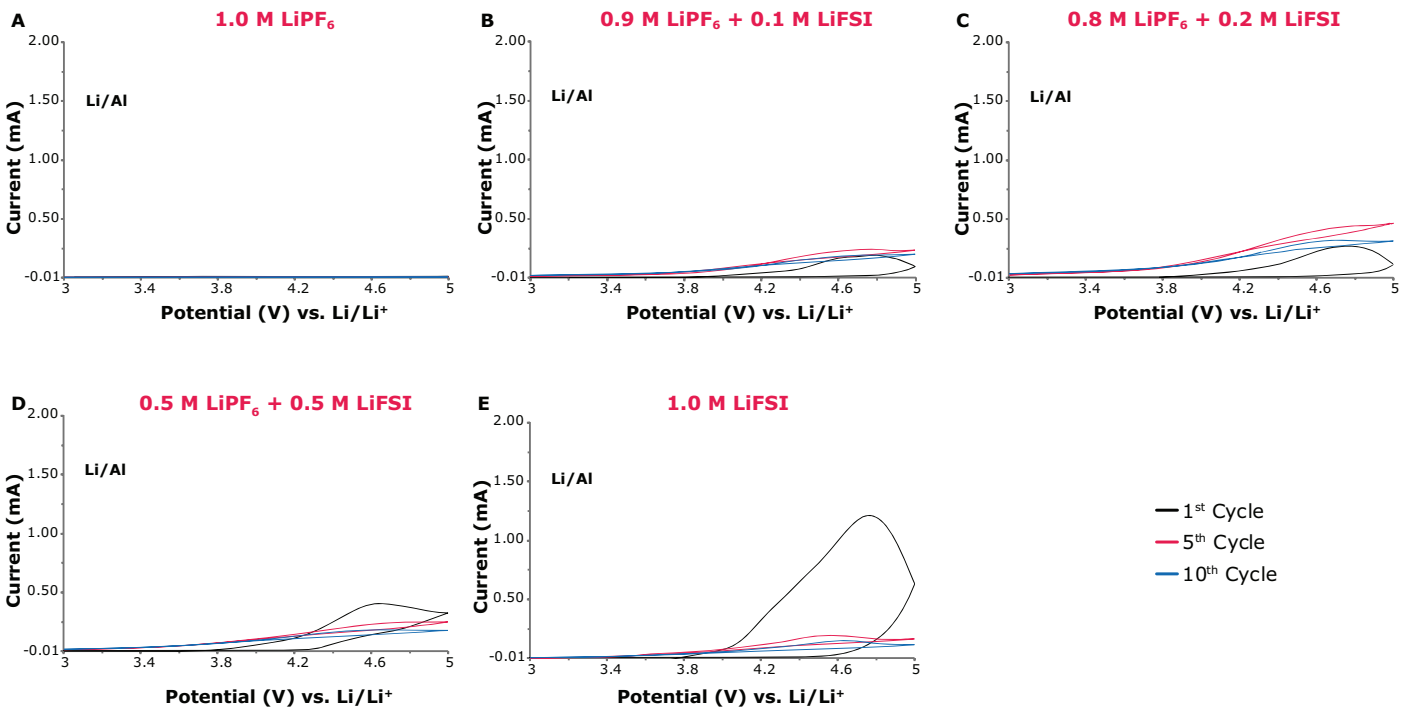

Figure 6. Cyclic voltammetry (CV) profiles for aluminum corrosion evaluation using lithium metal as both counter and reference electrodes in Li|electrolyte|Al cells. The 1st, 5th, and 10th CV cycles are shown for electrolytes with $LiPF_6$/LiFSI molar ratios of (**A**) 1.0 M $LiPF_6$, (**B**) 0.9 M $LiPF_6$ + 0.1 M LiFSI, (**C**) 0.8 M $LiPF_6$ + 0.2 M LiFSI, (**D**) 0.5 M $LiPF_6$ + 0.5 M LiFSI, and (**E**) 1.0 M LiFSI. Measurements were conducted in the potential window of 3.0–5.0 V vs. Li/Li^+ at a scan rate of 0.5 mV s^{-1}.

SEM analysis in **Figure 7** provides qualitative morphological context for electrochemical corrosion behavior. **Figure 7A** shows the pristine aluminum foil prior to electrochemical exposure. Following cycling, aluminum foils exposed to the 1.0 M $LiPF_6$ (**Figure 7B**) largely preserve a similar surface morphology, with no clear signs of localized corrosion. The low LiFSI composition (**Figure 7C**) also retains a relatively smooth surface with minimal visible surface disruption, closely resembling the 1.0 M $LiPF_6$ case. With increasing LiFSI content (**Figures 7D** and **7E**), subtle increases in surface roughness and isolated pit-like features become observable, suggesting the early stages of localized surface modification rather than extensive pitting. In contrast, the 1.0 M LiFSI (**Figure 7F**) leads to pronounced localized corrosion, characterized by large pits and cavities indicative of more aggressive aluminum dissolution. The comparatively mild morphological changes observed for the mixed-salt systems particularly at lower LiFSI content are consistent with their moderated corrosion currents, while also indicating that more pronounced surface evolution may develop with extended cycling under the tested conditions.

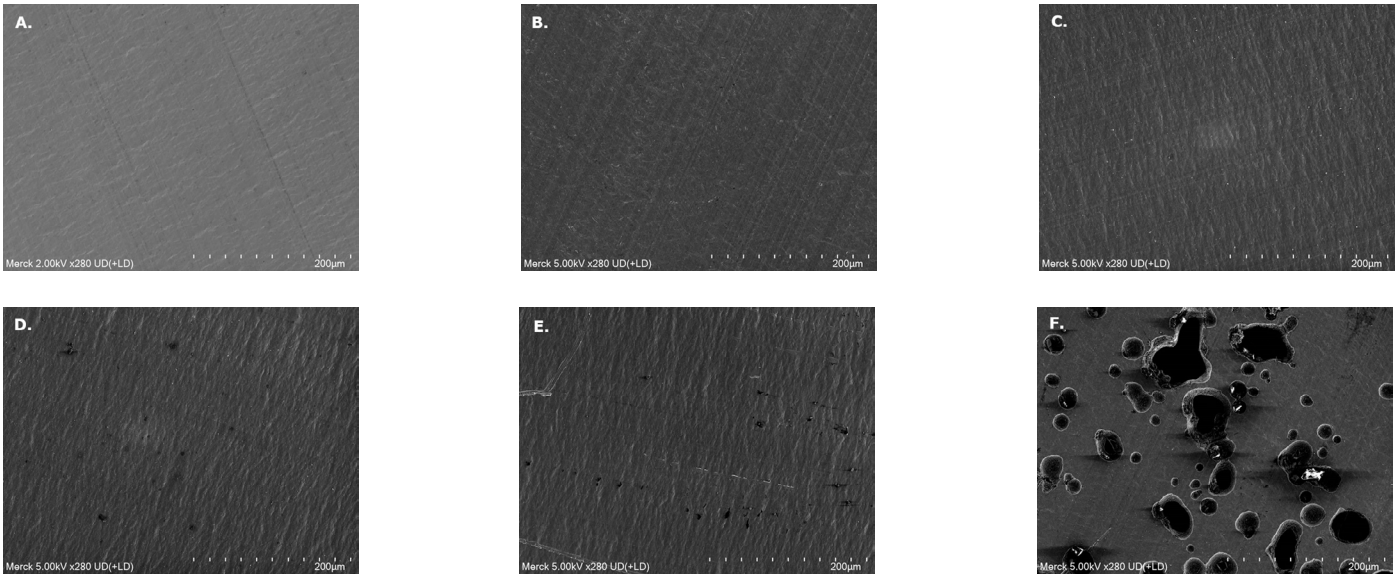

Figure 7. Scanning electron microscopy (SEM) images of aluminum (Al) foil surfaces after conducting electrochemical testing. Panel (**A**) shows pristine Al foil, while panels (**B–F**) show Al foils after five cyclic voltammetry (CV) scans in the potential window of 3.0–5.0 V vs. Li/Li^+ using $LiPF_6$/LiFSI electrolytes with the following molar ratios of (**B**) 1.0 M $LiPF_6$, (**C**) 0.9 M $LiPF_6$ + 0.1 M LiFSI, (**D**) 0.8 M $LiPF_6$ + 0.2 M LiFSI, (**E**) 0.5 M $LiPF_6$ + 0.5 M LiFSI, and (**F**) 1.0 M LiFSI.

The contrasting aluminum corrosion behaviors observed for $LiPF_6$- and LiFSI-based electrolytes arise from differences in how PF_6^- and FSI^- interact with the aluminum surface under anodic polarization. PF_6^- decompose to generate fluoride species that facilitate the formation of a thin, AlF_3 rich passivation layer, which limits aluminum dissolution, whereas FSI^- proceeds with formation of soluble Al(FSI) complexes that promote localized dissolution and pitting during polarization, as evidenced by both electrochemical measurements and surface morphology. Previous studies show that the presence of PF_6^- reduces aluminum current collector corrosion relative to imide-based anions and supports the formation of fluoride-rich surface films that more effectively suppress anodic attack.[18–20]

Linear sweep voltammetry (LSV) on aluminum (**Figure 8**) shows a monotonic reduction in oxidative stability with increasing LiFSI content, following the order 1.0 M $LiPF_6$ > 0.9 M $LiPF_6$ + 0.1 M LiFSI > 0.8 M $LiPF_6$ + 0.2 M LiFSI > 0.5 M $LiPF_6$ + 0.5 M LiFSI > 1.0 M LiFSI. This trend is consistent with the stronger passivation behavior of PF_6^- on aluminum, which delays anodic electrolyte oxidation, whereas FSI^- is less effective in maintaining surface stability under high potentials.

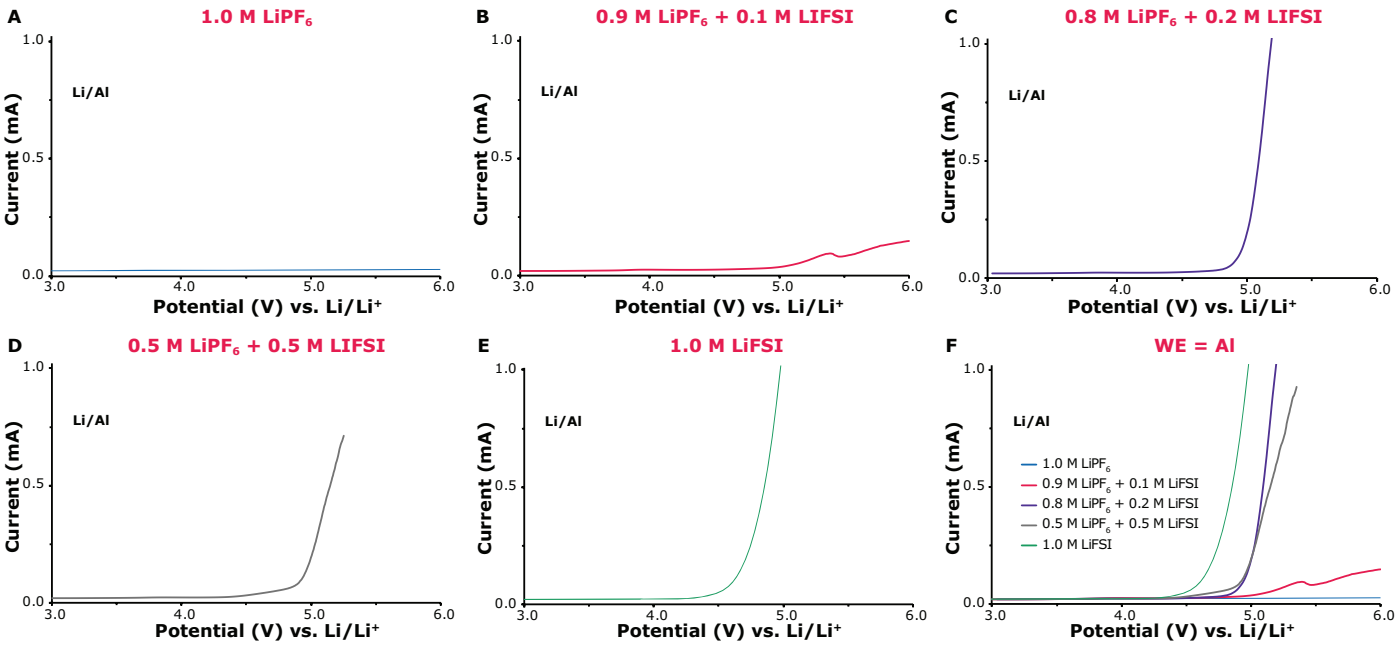

Figure 8. LSV profiles recorded using aluminum as the WE in Li|electrolyte|Al cells for $LiPF_6$/LiFSI electrolytes with molar ratios of (**A**) 1.0 M $LiPF_6$, (**B**) 0.9 M $LiPF_6$ + 0.1 M LiFSI, (**C**) 0.8 M $LiPF_6$ + 0.2 M LiFSI, (**D**) 0.5 M $LiPF_6$ + 0.5 M LiFSI, and (**E**) 1.0 M LiFSI. Panel (**F**) shows an overlay of the LSV curves from panels (**A–E**) plotted on a single graph for direct comparison. Measurements were performed at a scan rate of 0.5 mV s^{-1}.

On platinum electrodes (**Figure 9**), the oxidative stability trend shifts to 1.0 M $LiPF_6$ > 0.9 M $LiPF_6$ + 0.1 M LiFSI > 0.8 M $LiPF_6$ + 0.2 M LiFSI > 1.0 M LiFSI > 0.5 M $LiPF_6$ + 0.5 M LiFSI, reflecting the dominant role of electrode-catalyzed electrolyte oxidation. Unlike aluminum, platinum does not form a protective passivation layer; consequently, the observed oxidation behavior is governed primarily by the intrinsic reactivity of the electrolyte and catalytic decomposition pathways at the electrode surface. Under these conditions, LSV probes direct electron-transfer driven oxidation processes of the electrolyte, leading to stability rankings that differ from those observed on aluminum, where surface passivation strongly influences the apparent oxidative response.[21]

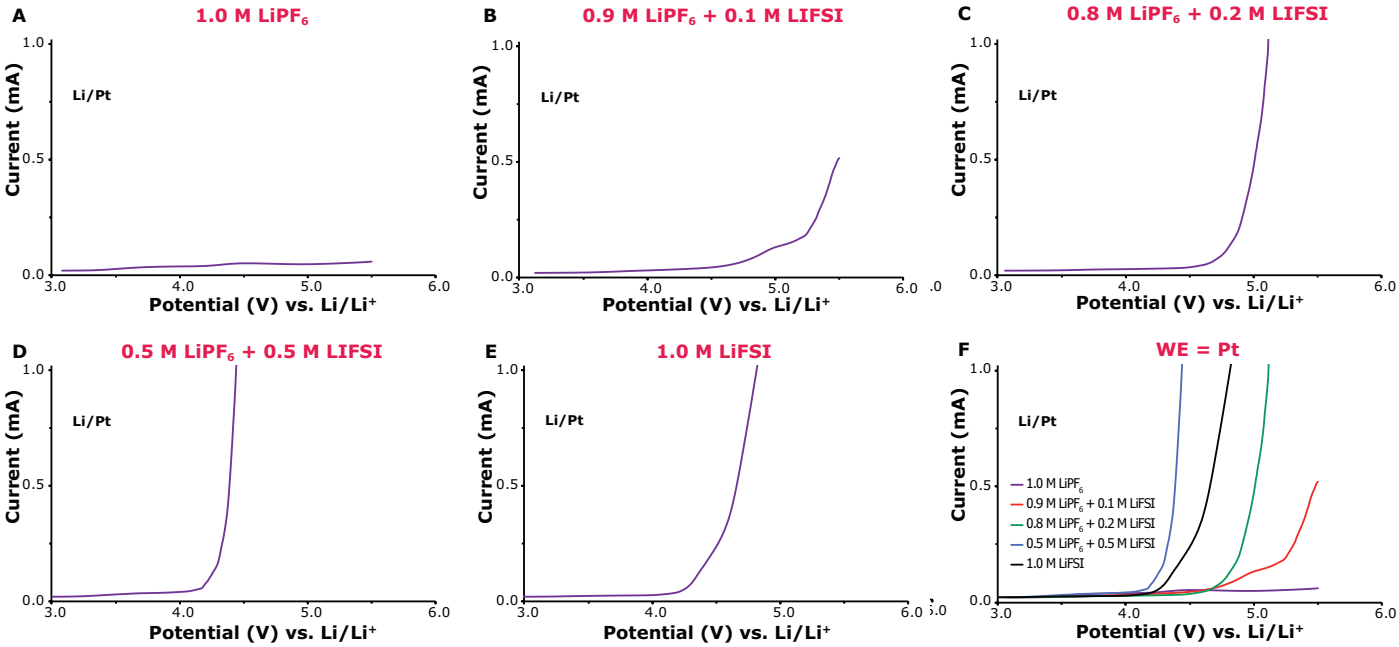

Figure 9. Linear sweep voltammetry (LSV) profiles recorded using platinum as the working electrode (WE) in Li|electrolyte|Pt cells for $LiPF_6$/LiFSI electrolytes with molar ratios of (**A**) 1.0 M $LiPF_6$, (**B**) 0.9 M $LiPF_6$ + 0.1 M LiFSI, (**C**) 0.8 M $LiPF_6$ + 0.2 M LiFSI, (**D**) 0.5 M $LiPF_6$ + 0.5 M LiFSI, and (**E**) 1.0 M LiFSI. Panel (**F**) presents an overlay of the LSV curves shown in panels (**A–E**) for direct comparison. All measurements were conducted at a scan rate of 0.5 mV s^{-1}.

SS electrodes (**Figure 10**) exhibit intermediate behavior, with oxidative stability following 1.0 M $LiPF_6$ > 0.9 M $LiPF_6$ + 0.1 M LiFSI > 0.8 M $LiPF_6$ + 0.2 M LiFSI ≈ 0.5 M $LiPF_6$ + 0.5 M LiFSI > 1.0 M LiFSI. The reduced distinction between mid-range salt compositions suggests comparable surface-controlled oxidation responses under the tested conditions, consistent with the partially passivating yet catalytically active nature of SS. In contrast to aluminum, the native oxide film on SS is less strongly influenced by electrolyte anion chemistry, while still providing a degree of surface moderation absent on platinum, resulting in oxidative trends that lie between passivation-dominated and purely catalytic regimes.[22,23]

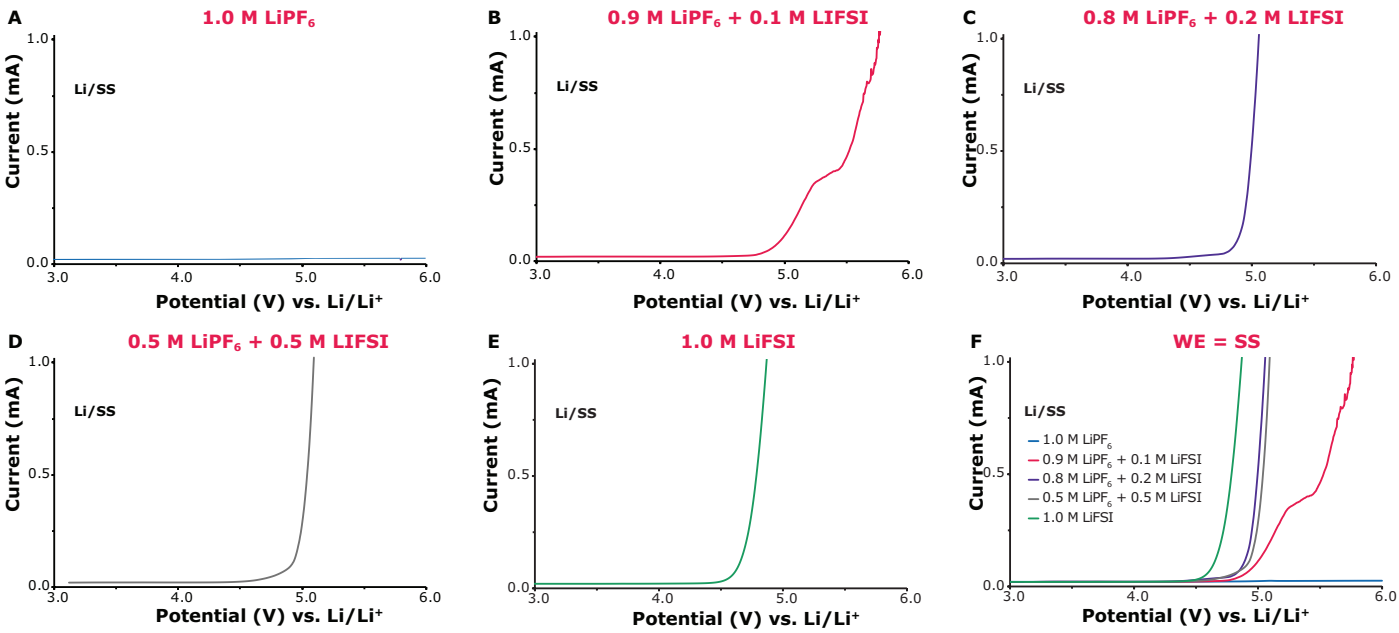

Figure 10. Linear sweep voltammetry (LSV) profiles recorded using SS as the working electrode in Li|electrolyte|SS cells for $LiPF_6$/LiFSI electrolytes with molar ratios of (**A**) 1.0 M $LiPF_6$, (**B**) 0.9 M $LiPF_6$ + 0.1 M LiFSI, (**C**) 0.8 M $LiPF_6$ + 0.2 M LiFSI, (**D**) 0.5 M $LiPF_6$ + 0.5 M LiFSI, and (**E**) 1.0 M LiFSI. Panel (**F**) shows the overlaid LSV curves from panels (**A–E**) plotted together for direct comparison. Measurements were carried out at a scan rate of 0.5 mV s^{-1}.

Conclusion

This study systematically evaluated $LiPF_6$- and LiFSI-based electrolyte salts from our catalog, with a focus on transport properties, lithium metal interfacial behavior, and anodic stability across relevant electrode materials. This comprehensive electrochemical assessment provides a data-driven basis for electrolyte salt selection. Electrochemical testing showed that mixed-salt electrolytes incorporating moderate concentrations of LiFSI (0.2 M) into $LiPF_6$-based electrolytes enhanced ionic conductivity, lithium-ion transference, and lithium plating/stripping reversibility compared to the 1.0 M $LiPF_6$ formulations. However, these performance gains were accompanied by a progressive reduction in anodic stability on aluminum with increasing LiFSI content. Among the evaluated compositions, mixed-salt electrolytes offered a balanced performance window by moderating aluminum corrosion while retaining many of the transport and interfacial benefits associated with LiFSI, supporting their use in applications requiring tailored trade-offs between conductivity, lithium stability, and current collector compatibility.

Featured Products

Description	Cat. No.
Lithium bis(fluorosulfonyl)imide, 99.9% trace metals basis, battery grade	**935832**
Lithium hexafluorophosphate, battery grade, ≥99.99% trace metals basis	**450227**
Ethylene carbonate, battery grade, ≥99%, acid <10 ppm, H_2O <10 ppm	**809950**
Dimethyl carbonate, battery grade, ≥99.9%, acid <10 ppm, H_2O <10 ppm	**809942**
Platinum, foil, thickness 0.025 mm, 99.9% trace metals basis	**267244**
Stainless Steel – AISI 420 alloy, $Fe_{86.7}Cr_{13.0}C_{0.3}$, foil, 100 x 100 mm, 0.075 mm thickness, annealed, light tight (lt)	**GF77425274**

Related Products

Description	Cat. No.
Lithium bis(trifluoromethanesulfonyl)imide, 99.99% trace metals basis	**919977**
Lithium tetrafluoroborate, ultra dry, powder, 99.99% trace metals basis	**451622**
LiTDI, powder, ≥99.9% trace metals basis, battery grade	**940496**
LiBETI, electrolyte powder, anhydrous, battery grade	**940186**
Lithium bis(oxalato)borate, Greener alternative	**757136**
Lithium difluoro(oxalato)borate, Greener alternative	**774138**
Lithium perchlorate, battery grade, dry, 99.99% trace metals basis	**634565**
Ethyl methyl carbonate, 99%	**754935**
Propylene carbonate, battery grade, ≥99%, acid <10 ppm, H_2O <10 ppm	**809969**
Diethyl carbonate, battery grade, ≥99%, acid <10 ppm, H_2O <10 ppm	**900018**
Lithium hexafluorophosphate solution, in ethylene carbonate and dimethyl carbonate, 1.0 M $LiPF_6$ in EC/DMC = 50/50 (v/v), battery grade	**746711**

For more information visit us at
SigmaAldrich.com/battery

References

1. Valøen, L. O.; Reimers, J. N. Transport Properties of $LiPF_6$ Based Li Ion Battery Electrolytes. *J. Electrochem. Soc.* **2005**, *152*, A882 – A891. DOI: **10.1149/1.1872737**
2. Xu, K. Electrolytes and Interphases in Li Ion Batteries and Beyond. *Chem. Rev.* **2014**, *114*, 11503–11618. DOI: **10.1021/cr500003w**
3. Li, S.; Zhu, K.; Yang, Y.; Wu, L.; Wang, J.; Xu, H.; He, X. Unraveling the Hydrolysis Mechanism of $LiPF_6$ in Electrolyte of Lithium Ion Batteries. *Nano Lett.* **2024**, *24* (2). DOI: **10.1021/acs.nanolett.3c01682**
4. Stich, M.; Göttlinger, M.; Kurniawan, M.; Schmidt, U.; Bund, A. Hydrolysis of $LiPF_6$ in Carbonate Based Electrolytes for Lithium Ion Batteries and in Aqueous Media. *J. Phys. Chem. C.* **2018**, *122* (16), 8705–8714. DOI: **10.1021/acs.jpcc.8b02080**
5. Qian, J.; Henderson, W. A.; Xu, W.; Bhattacharya, P.; Engelhard, M.; Borodin, O.; Zhang, J. G. High Rate and Stable Cycling of Lithium Metal Anode. *Nat. Commun.* **2015**, *6*, 6362. DOI: **10.1038/ncomms7362**
6. Berhaut, C. L.; Lemordant, D.; Porion, P.; Timperman, L.; Schmidt, G.; Anouti, M. Ionic Association Analysis of LiTDI, LiFSI, and $LiPF_6$ in EC/DMC for Improved Li Ion Battery Performance. *RSC Adv.* **2019**, *9* (8), 4599–4608. DOI: **10.1039/C8RA08430K**
7. Mwemezi, M.; Prabakar, S. J. R.; Han, S. C.; Seo, J. Y.; Park, W. B.; Lee, J. W.; Sohn, K. S.; Pyo, M. Dendrite Free Reversible Li Plating/Stripping in Adiponitrile Based Electrolytes for High Voltage Li Metal Batteries. *J. Mater. Chem. A.* **2021**, *9*, 4962–4970. DOI: **10.1039/D0TA12124J**
8. Wu, X.; Du, Z. Study of the Corrosion Behavior of LiFSI Based Electrolytes for Li Ion Cells. *Electrochem. Commun.* **2021**, *129*, 107088. DOI: **10.1016/j.elecom.2021.107088**
9. Wang, D. Y.; Xiao, A.; Wells, L.; Dahn, J. R. Effect of Mixtures of Lithium Hexafluorophosphate ($LiPF_6$) and Lithium Bis(fluorosulfonyl) imide (LiFSI) as Salts in $Li[Ni_{1/3}Mn_{1/3}Co_{1/3}]O_2$/Graphite Pouch Cells. *J. Electrochem. Soc.* **2015**, *162* (1), A169. DOI: **10.1149/2.0821501jes**
10. Zhang, L.; Chai, L.; Zhang, L.; Shen, M.; Zhang, X.; Battaglia, V. S.; Stephenson, T.; Zheng, H. Synergistic Effect Between Lithium bis(fluorosulfonyl)imide (LiFSI) And Lithium bis-oxalato borate (LiBOB) Salts in $LiPF_6$-Based Electrolyte for High-Performance Li-Ion Batteries. *Electrochim. Acta.* **2014**, *127*, 39–44. DOI: **10.1016/j.electacta.2014.02.008**
11. Evans, J.; Vincent, C. A.; Bruce, P. G. Electrochemical Measurement of Transference Numbers in Polymer Electrolytes. *Electrochim. Acta.* **1987**, *32*, 1097–1102. DOI: **10.1016/0032–3861(87)90394–6**
12. Xu, K. Navigating the Minefield of Battery Literature. *Commun. Mater.* **2022**, *3*, 31. DOI: **10.1038/s43246-022–00251-5**
13. Zugmann, S.; Fleischmann, M.; Amereller, M.; Gschwind, R. M.; Wiemhöfer, H. D.; Gores, H. J. Measurement of Transference Numbers for Lithium Ion Electrolytes via Four Different Methods, A Comparative Study. *Electrochim. Acta.* **2011**, *56*, 3926–3933. DOI: **10.1016/j.electacta.2011.02.025**
14. Wang, M.; Huai, L.; Hu, G.; Yang, S.; Ren, F.; Wang, S.; Zhang, Z.; Chen, Z.; Peng, Z.; Shen, C. Effect of LiFSI Concentrations to Form Thickness- and Modulus-Controlled SEI Layers on Lithium Metal Anodes. *J. Phys. Chem. C.* **2018**, *122* (18). DOI: **10.1021/acs.jpcc.8b02314**
15. Xu, R.; Yan, C.; Huang, J. Q. Competitive Solid–Electrolyte Interphase Formation on Working Lithium Anodes. *Trends Chem.* **2021**, *3* (1), 5–14. DOI: **10.1016/j.trechm.2020.10.008**
16. Leung, K.; Soto, F.; Hankins, K.; Balbuena, P. B.; Harrison, K. L. Stability of Solid Electrolyte Interphase Components on Lithium Metal and Reactive Anode Material Surfaces. *J. Phys. Chem. C.* **2016**, *120* (12). DOI: **10.48550/arXiv.1605.07142**
17. Piao, Z.; Han, Z.; Tao, S.; Zhang, M.; Lu, G.; Su, L.; Wu, X.; Song, Y.; Xiao, X.; Zhang, X.; Zhou, G.; Cheng, H. M. Deciphering Failure Paths in Lithium Metal Anodes by Electrochemical Curve Fingerprints. *Natl. Sci. Rev.* **2025**, *12* (7), nwaf158. DOI: **10.1093/nsr/nwaf158**
18. Du, P.; Wan, J.; Qu, J.; et al. Passivation and Corrosion of Al Current Collectors in Lithium Ion Batteries. *npj Mater. Degrad.* **2024**, *8*, 43. DOI: **10.1038/s41529-024–00453-x**
19. Scheer, K. M.; Tulloch, M.; Hamam, I.; Abraham, J. J.; Johnson, M. B.; Metzger, M. Anodic Dissolution of the Aluminum Current Collector in Lithium-ion Cells with LiFSI, $LiPF_6$, and $LiBF_4$. *J. Electrochem. Soc.* **2025**, *172* (1), 010511. DOI: **10.1149/1945–7111/ada641**
20. Cho, E.; Mun, J.; Chae, O. B.; Kwon, O. M.; Kim, H. T.; Ryu, J. H.; Kim, Y. G.; Oh, S. M. Corrosion and Passivation of Aluminum Current Collectors in Bis(fluorosulfonyl)imide Based Ionic Liquid for Lithium-ion Batteries. *Electrochim. Acta.* **2012**, *82*, 1–7. DOI: **10.1016/j.elecom.2012.05.018**
21. He, R.; McDonough, L.; Seitz, L.; Ou, W.; Marks, S.; Ferreira de Menezes, R.; Allan Cole, E.; Luo, H.; Toney, M.; Sprenger, K.; Zhou, M.; Tenent, R. In Situ Characterization of the Oxidation Behavior of Carbonate-Based Electrolytes for Lithium-Ion Batteries by Scanning Electrochemical Microscopy. *ACS Electrochem.* **2025**, *1* (4), 494–503. DOI: **10.1021/acselectrochem.4c00106**
22. Choi, S. H.; Yoo, Y. R.; Kim, Y. S. Semiconductive Tendency of Passive Films on Super Austenitic Stainless-Steel SR-50A in Acidic or Alkaline Chloride Solutions. *Crystals.* **2024**, *14* (9), 766. DOI: **10.3390/cryst14090766**
23. Sengeni, A.; Sato, H.; Suguru, N. Chemical Leaching of Inactive Cr and Electrochemical Resurfacing of Catalytically Active Sites in Stainless Steel for High-Rate Alkaline Hydrogen Evolution Reaction. *ACS Appl. Energy Mater.* **2020**, *3* (12), 12596–12606. DOI: **10.1021/acsaem.0c02505**

To place an order or receive technical assistance:
SigmaAldrich.com/support

For local contact information:
SigmaAldrich.com/offices

Merck KGaA
Frankfurter Strasse 250
64293 Darmstadt, Germany

SigmaAldrich.com

We have built a unique collection of life science brands with unrivalled experience in supporting your scientific advancements.

Millipore® Sigma-Aldrich® Supelco® Milli-Q® SAFC® BioReliance®

© 2026 Merck KGaA, Darmstadt, Germany and/or its affiliates. All Rights Reserved. Merck, the vibrant M, BioReliance, Millipore, Milli-Q, SAFC, Sigma-Aldrich and Supelco are trademarks of Merck KGaA, Darmstadt, Germany or its affiliates. All other trademarks are the property of their respective owners. Detailed information on trademarks is available via publicly accessible resources.

MK_AN14342EN Ver. 1.0 70949 09/2026